

Morphology of an asymmetric ethyleneoxide–butadiene di-block copolymer in bulk and thin films

Denitza M. Lambreva^a, Ricarda Opitz^a, Günter Reiter^b, Peter M. Frederik^c, Wim H. de Jeu^{a,*}

^aResearch Group Order/Disorder in Soft Matter, FOM-Institute for Atomic and Molecular Physics, Kruislaan 407, 1098 Amsterdam, The Netherlands

^bInstitut de Chimie des Surfaces et Interfaces, CNRS-UHA, BP 2488, F-68057 Mulhouse, France

^cDepartment of Pathology, Electron Microscopy, University of Limburg, Maastricht, The Netherlands

Received 23 November 2004; received in revised form 15 February 2005; accepted 25 February 2005

Available online 19 April 2005

Abstract

We present experiments on the melt and crystal morphology of an asymmetric semi-crystalline poly(ethylene/butylene-*b*-ethyleneoxide) diblock copolymer (PB_n-*b*-PEO) in bulk as well as in thin films. Simultaneous small- and wide-angle X-ray scattering combined with AFM and TEM images reveal in the melt a bulk morphology of hexagonally packed cylinders of PEO in a PB_n matrix, that transforms into a hexagonal perforated lamellar phase upon crystallization. X-ray reflectivity of thin films of PB_n-*b*-PEO in the melt indicates wetting layers at the top and bottom interfaces, which force the cylinders in the interior to orient parallel to the substrate. Crystallization of the PEO block leads to roughening of the air/film interface and causes lateral structuring coexisting with planar lamellar layers in thinner films.

© 2005 Elsevier Ltd. All rights reserved.

Keywords: Semicrystalline–amorphous block copolymers; Phase behavior; Scattering

1. Introduction

Semicrystalline–amorphous block copolymers provide unique opportunities to examine the interplay of various types of phase transitions, resulting in a rich phase behavior and molecular ordering over several length scales. Below the order–disorder transition at a temperature T_{ODT} micro-phase separation drives the formation of nanoscale lamellae, cylinders or other structures, depending on the degree of incompatibility (Flory–Huggins parameter χ) and the volume fractions of the A- and B-blocks [1]. However, upon crystallization of one of the blocks the development of crystalline lamellae is favoured [2–4]. These processes depend strongly on the particular morphology, the degree of supercooling and the nature of the confinement [5,6]. In particular when T_{ODT} and the melting temperature T_m are close, competition and coupling between the micro-phase separation and crystallization can occur [7]. In this paper, we concentrate on small deviations from lamellar micro-

phase separation for which situation coupling with crystallization can also be expected to be strong.

Lamellar diblock copolymers consisting of an amorphous poly(ethylene/butylene) block and a crystallisable polyethyleneoxide block, indicated as BE or PB_n-PEO, have been extensively studied as model systems for confined crystallization [8]. In thin films of B₃₇₀₀E₄₃₀₀ with an approximately symmetric composition (*E* volume fraction 47%) the lamellae orient parallel to the substrate, which results in many orders of Bragg peaks in X-ray reflectivity measurements [9]. Interestingly, crystallization of the PEO-block causes an increase of the lamellar block period such that the PEO sub layer thickness allows (half) integer chain folding. Due to this expansion and the associated increase in density of PEO, lateral contraction is needed to conserve mass, leading to cracks through the whole film. The slightly more asymmetric diblock B₃₇₀₀E₂₉₀₀ (*E* volume fraction 37%, in short BE37) revealed a rather different bulk and surface behaviour than various more symmetric compounds [10,11]. In thin films optical observations gave island-hole patterns with a step height equal to the expected thickness of block lamellae parallel to the substrate while for specific supercooling a unique structure of lamellae perpendicular to the substrate was found. In this paper we focus on the morphology of BE37 in

* Corresponding author.

the molten and crystalline state. Simultaneous small- and wide-angle X-ray scattering (SAXS/WAXS) experiments combined with AFM and TEM images, reveal in the melt a bulk morphology of hexagonally packed cylinders (HPC) of PEO in a PB_h matrix, that most probably transforms into a hexagonally perforated lamellar (HPL) phase upon crystallization. Films on a substrate behave somewhat differently: X-ray reflectivity indicates that wetting layers develop at the top and bottom interface. This forces the remaining cylinders in the middle of the film to become parallel to the substrate. Crystallization of the PEO cylinders with lamellae perpendicular to the block interfaces then could lead to crystalline lamellae perpendicular to the film surface as observed.

2. Experimental section

2.1. Materials

Poly(ethylene/butylene-*b*-ethyleneoxide) (BE37) was obtained from Goldschmidt AG (Germany). Synthesis was done by sequential anionic polymerization of ethylene oxide and butadiene (about equal amounts of 1,2 and 1,4 units, statistically distributed). The resulting copolymer consists of an OH-terminated PEO-block and a hydrogenated polybutadiene block (PB_h). Details of the molecular characteristics in the melt are given in Table 1. The molecular volume V_{mol} of each of the blocks was calculated using $V_{\text{mol}} = M_n / (\rho N_A)$, in which N_A is Avogadro's number and ρ the density of the particular block. Then the volume fraction PEO simply follows from $f_E = V_{\text{mol}}^E / (V_{\text{mol}}^E + V_{\text{mol}}^B)$. We used values for the density of the PEO and PB_h blocks 1.13 and 0.86 g/cm³, respectively. Upon crystallization the density ρ_{PEO} changes to about 1.23 g/cm³. The bulk melting temperature is around 57 °C [11]. Prior to use the polymer was dried under vacuum at 80 °C to remove any residual solvent.

2.2. Small and wide-angle X-ray scattering

Simultaneous SAXS and WAXS measurements were performed using an in-house set-up with a rotating anode X-ray generator (Rigaku RU-H300, 18 kW). A monochromatic beam (wavelength $\lambda = 0.154$ nm) with a divergence about 0.012° was acquired using two parabolic multilayer

mirrors (Bruker, Karlsruhe, Germany). The SAXS and WAXS intensities were recorded by a two-dimensional (Bruker Hi-Star) and linear (PSD-50M, M. Braun) detector, respectively. The collected data were azimuthally integrated and corrected for the geometry of the scattering entities ('Lorentz correction'). Graphically the relative intensity is presented vs $q = (4\pi/\lambda)\sin\theta$, where q is the modulus of the wave vector transfer and 2θ is the scattering angle.

2.3. X-ray reflectivity

X-ray reflectivity measurements were carried out using a two-circle diffractometer attached to the same rotating anode generator. The incident beam was monochromatized to $\lambda = 0.154$ nm (Cu K α -line) and collimated to 0.025° in the horizontal scattering plane (xz -plane with the z -axis along the film normal) by a W/B₄C graded parabolic multilayer mirror (Osmic, Auburn Hills, USA). Additional pre-sample and pre-detector slits lead to an overall in-plane resolution given by $\Delta q_z = 0.043$ nm⁻¹ and $\Delta q_x = 5 \times 10^{-3} q_z$.

In reciprocal space specular reflectivity scans probe the scattered intensity along q_z . The X-ray intensity was corrected for sample size effects at small incidence angles as well as for background scattering; the incident intensity was normalized to unity. The data were analyzed using an iterative matrix formalism derived from the Fresnel equations, taking the deviations from the ideal decay of the reflectivity for a perfectly smooth surface due to the presence of roughness into account [12]. The calculated reflectivity profiles were convoluted with the experimental resolution, assumed to be of Gaussian statistics.

2.4. Atomic force microscopy (AFM)

Height and phase images of the crystalline morphology of the diblock copolymers were taken using a Solver AFM from NT-MDT (Zelenograd, RF) at ambient conditions in the tapping mode. A vibrating cantilever with a resonant frequency of about 300 kHz and a silicon tip with a radius of curvature less than 10 nm were used. To examine the bulk crystalline morphology by AFM the crystallized samples were quenched in liquid nitrogen and cut. As discussed earlier [7] in this way surfaces smooth enough for AFM imaging can be obtained that reflect the bulk morphology.

2.5. Transmission electron microscopy (TEM)

Cryo-sections were obtained from bulk BE45 and observed at low temperatures in the electron microscope using low-dose conditions for imaging. A small part of the sample (less than a cubic mm) was mounted on a silver pin, frozen by dropping into liquid nitrogen and mounted in a Leica Ultracut S (Vienna, Austria) equipped with an FCS attachment for low temperature sectioning. At -70 °C thin sections were cut on a 'dry' diamond knife. Smooth sections were collected with a dry eyelash probe and pressed by hand

Table 1
Molecular characteristics of BE37 in the melt

| | PEO | PB _h |
|--|------|-----------------|
| M_n (g/mol) | 2900 | 3700 |
| Number of monomers N | 66 | 66 |
| Volume fraction f | 0.37 | 0.63 |
| Radius of gyration $R_G = a\sqrt{(N/6)}$ | 0.93 | 1.28 |
| Length of non-folded block (nm) | 18.5 | 25.4 |
| Polydispersity | 1.1 | |

onto the carbon coated formvar supporting film of a specimen grid. The grids were transferred to the cryo-holder (Gatan 626, Pleasanton, CA, USA) of the CM12 microscope (Philips, Eindhoven, The Netherlands) using the cryo-transfer station. During observation and imaging the temperature was kept at $-170\text{ }^{\circ}\text{C}$ to minimize beam damage.

2.6. Samples preparation and measurement procedure

For SAXS the polymer was put between two pieces of a Kapton foil separated by a metal ring fixing the thickness to about 0.5 mm. A Linkam CSS450 temperature-controlled shear system was used as sample holder. In order to probe the polymer morphology in the melt we initially kept the sample at $90\text{ }^{\circ}\text{C}$ for 10 min and then cooled it down to $40\text{ }^{\circ}\text{C}$. Subsequently, we increased the temperature and took SAXS scans at various temperatures up to $300\text{ }^{\circ}\text{C}$. To study bulk crystallization again each sample was kept at $90\text{ }^{\circ}\text{C}$ for 10 min and then cooled to the crystallization temperature T_{cr} at about $10\text{ }^{\circ}\text{C}/\text{min}$. The SAXS and WAXS signals were monitored simultaneously in order to track the crystallization process. The measurements were done in a dry nitrogen atmosphere and no degradation effects were observed during the annealing at $90\text{ }^{\circ}\text{C}$.

Thin films were prepared by spin-coating low-concentration solutions of BE37 in dichloromethane (DCM) on a silicon wafer at 2000 rpm. The wafers were first cleaned in chromic acid for about 10 min and then rinsed in ultra-pure water. During X-ray reflectivity measurements the sample was kept in a two-stage oven regulated within $0.1\text{ }^{\circ}\text{C}$ by a Eurotherm controller and evacuated to $\sim 10^2\text{ Pa}$. The films were annealed at $T_{\text{ann}}=90\text{ }^{\circ}\text{C}$ and then cooled down to T_{cr} at about $10\text{ }^{\circ}\text{C}/\text{min}$.

3. Results

3.1. Bulk ordering

Fig. 1 shows SAXS patterns from the BE37 melt upon heating from 40 to $300\text{ }^{\circ}\text{C}$. At all temperatures the polymer remains phase separated, hence T_{ODT} is well above $300\text{ }^{\circ}\text{C}$. Pronounced scattering peaks appear at relative positions $1:3^{1/2}:4^{1/2}:7^{1/2}:12^{1/2}:13^{1/2}$ as illustrated for $48\text{ }^{\circ}\text{C}$ in the top curve of Fig. 2. This assignment corresponds to hexagonal lattice constant $a=4\pi/(3^{1/2}q_{100})$ varies from 16 nm around $300\text{ }^{\circ}\text{C}$ to 22.7 nm at $48\text{ }^{\circ}\text{C}$ (see inset Fig. 1). Upon increasing the temperature the intensity of some of the peaks decreases or completely vanishes, reflecting smearing of the density profile and broadening of the interfaces. Based on the values for the volume fractions [13] the relevant diblock copolymer morphology is assumed to consist of hexagonally packed cylinders of PEO in a matrix of the majority component PB_h . This conclusion differs from the assumption of a lamellar phase given in Ref. [11]

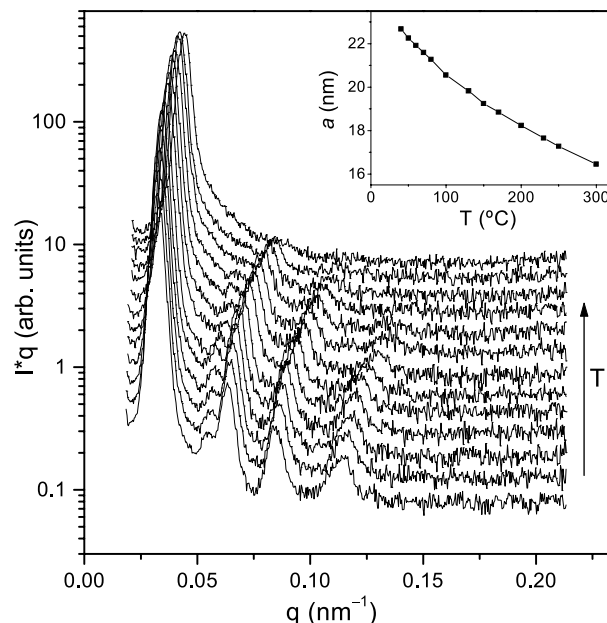


Fig. 1. SAXS profiles of BE37 in molten state at various temperatures (from bottom to top: $40\text{--}80$ (with $10\text{ }^{\circ}\text{C}$ step), $100, 130, 150, 170, 200, 250, 300\text{ }^{\circ}\text{C}$). The curves are shifted for clarity and indicate hexagonal symmetry. The inset presents the hexagonal lattice parameter $a=4\pi/(3^{1/2}q_{100})$ as a function of temperature.

on the basis of optical observations in films. Interestingly in Ref. [11], BE37 is reported to behave rather differently compared to several more symmetric lamellar BE block copolymers. This is in agreement with our assignment of a hexagonal phase on the basis of unambiguous SAXS data.

Upon crystallization the scattering profiles change considerably, see Fig. 2. The reference curve from the

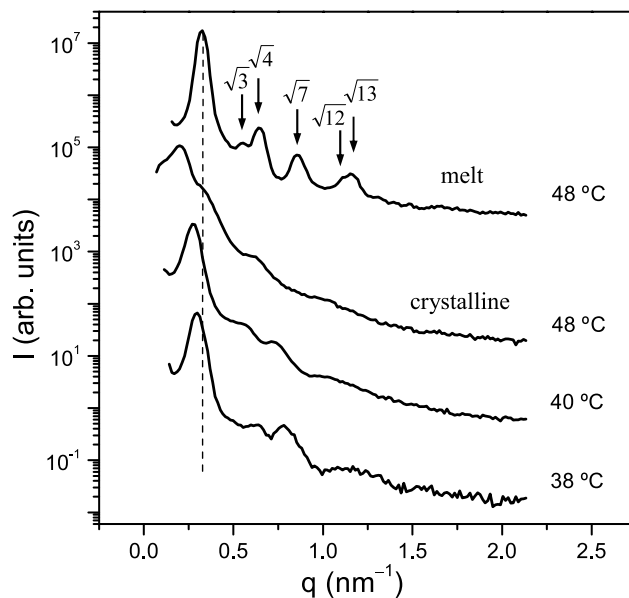


Fig. 2. SAXS profiles of BE37 crystallized at various temperatures. The melt morphology at $48\text{ }^{\circ}\text{C}$ from Fig. 1 is shown for comparison. The curves are shifted for clarity.

melt morphology at 48 °C ($a=22.7$ nm) represents also the melt at 38 and 40 °C, since the difference in the intercylinder distance at these temperatures is only a few tenth of nanometer. The sample crystallized at 38 °C gives pronounced peaks at 0.29, 0.58 and 0.77 nm⁻¹. The ratio 1:4^{1/2}:7^{1/2} of their positions agrees with a hexagonally packed structure with $a=25$ nm. Increasing T_{cr} results in similar scattering profiles. At 40 °C the peaks are positioned at 0.27, 0.55 and 0.72 nm⁻¹, respectively, again at 1, 4^{1/2} and 7^{1/2} times the fundamental wave vector corresponding to $a=26.9$ nm. The SAXS curve taken at $T_{cr}=48$ °C comprises contributions from both the crystalline morphology and the residual melt structure. On the time scale of the experiment (3 days) the first-order melt peak did not disappear fully. Reflections from the crystallized part at 0.21 and 0.56 nm⁻¹ (1:7^{1/2}) reveal hexagonal symmetry with $a=34.5$ nm. The peak corresponding to $2q_{100}$ is probably hidden in the residual first-order molten peak.

To determine the morphology associated with the hexagonal symmetry in the crystallized BE37, we performed AFM on a surface of the bulk polymer crystallized at 48 °C obtained by cryogenic microtomography. A typical picture presented in Fig. 3(a) shows elongated structures that could in principle be lamellae or cylinders. However, in the case of cylinders we would also expect approximately hexagonal ‘head-on’ structures that were not observed. In addition lateral modulations are seen along the elongated structures with a period of about 25–30 nm, which are neither expected for cylinders nor for lamellae. Other parts of the sample show only small variations in the phase contrast and can be conceived as domains with different orientation. Supplementary TEM measurements on unstained BE37 samples crystallized at 48 and 40 °C (Fig. 3(b)) corroborate the modulations seen in AFM. In Ref. [7]

very similar modulations were seen in cryocut block copolymers, which could unambiguously be related to perforated lamellae by SAXS on an oriented sample. Analogous to these observations we interpret them here in BE37 also as perforations of lamellae, characteristic of the HPL phase.

3.2. Ordering in thin films

To perform X-ray reflectivity measurements on thin films of BE37 samples were prepared from 0.3, 0.5, 1 and 2% solutions in DCM, to be referred to as films A, B, C and D with a thickness of the order of 20, 40, 80 and 140 nm, respectively. Examination by optical microscopy indicates that in the molten state the surface is covered with terraces (Fig. 4). After crystallization additional grain-like structures appear, which cause roughening of the air interface. In contrast to lamellar BE films, no crystallization front of pits and cracks [9,11] is observed during this process. Though the formation of terraces is typical of lamellar films, they are not restricted to this structure. They have also been observed for both cylindrical and spherical morphologies in thin films when the initial film thickness was not commensurable with the domain spacing [14]. Therefore, these features in films of BE37 are compatible with the HPC phase observed in bulk. AFM images of the crystallized thicker samples C and D display the perpendicular lamellae observed earlier by Reiter et al. [10]. However, the thinner films A and B show a hole/island topography (Fig. 5). Interestingly, the phase pictures reveal layers parallel to the surface coexisting with islands comprising perpendicular lamellae (Fig. 5(b) and (c)).

To obtain a more quantitative picture of the thin film morphology we performed X-ray reflectivity of both the

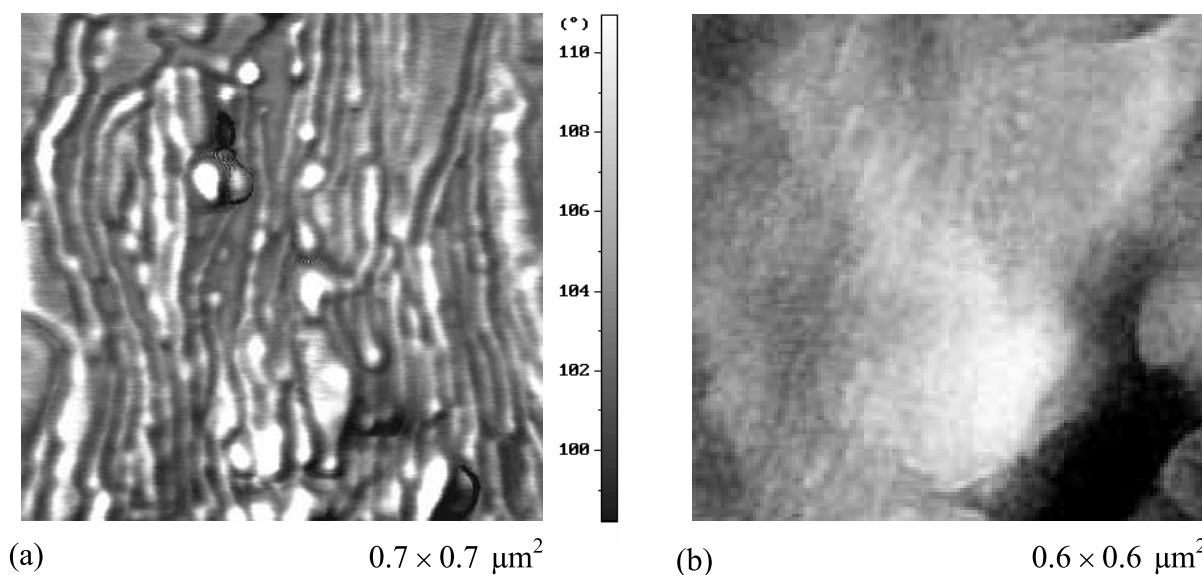


Fig. 3. Tapping mode AFM phase image (a) and non-stained TEM image (b) of bulk BE37 crystallized at 48 °C. The elongated lamellar patterns are modulated with a lateral period of 25–30 nm.

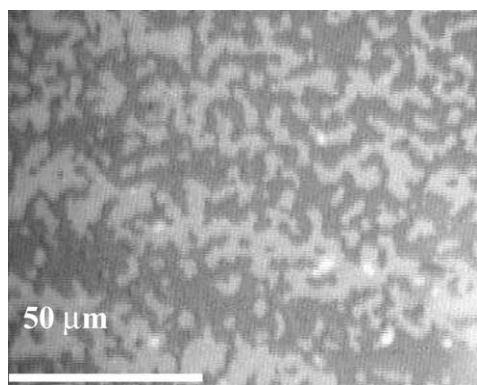


Fig. 4. Optical microscopy image of the surface topography of a BE37 film spin-coated from 2% DCM solution (sample D). Molten state at $T=90^\circ\text{C}$ with terrace-like height variations.

molten and the crystalline state (Fig. 6). The reflectivity curves are modulated by Kiessig fringes with a period $\Delta q_z = 2\pi/\lambda$, in which λ is the film thickness. The crystallized samples show smeared oscillations that reflect the roughening seen by optical microscopy. The observed beating in the melt of samples C and D corresponds to discrete height levels on the surface with $\Delta\lambda=18\text{--}19\text{ nm}$. None of the curves displays Bragg peaks as found in lamellar $\text{B}_{3700}\text{E}_{4300}$ films [9], excluding once more a regular planar lamellar morphology for the film structure.

4. Discussion

The results from bulk BE37 indicate a melt morphology of hexagonally packed cylinders. From the combination of SAXS and AFM/TEM images we conclude that in the bulk upon crystallization the HPC phase of the amorphous melt most probably transforms into a HPL phase. A HPL phase gives two fundamental X-ray reflections corresponding to the layer structure and the hexagonal perforations, respectively. From simple geometrical considerations their positions differ for a simple ABAB... stacking by a factor $2/\sqrt{3}$

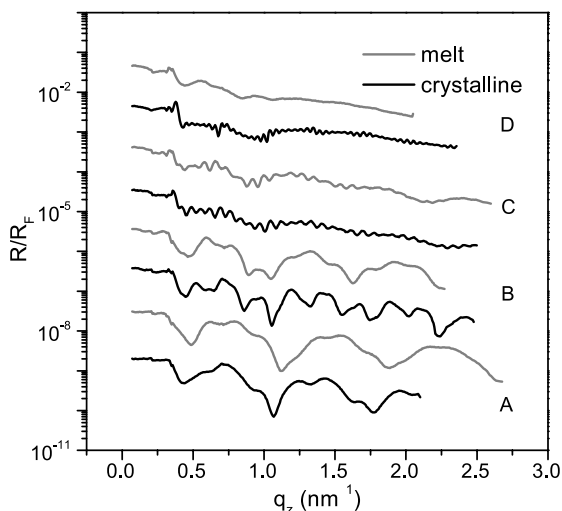


Fig. 6. Pairs of specular X-ray reflectivity curves of BE37 thin films at 90°C (melt) and 35°C (crystalline), respectively. A, B, C, D indicate the sample in increasing thickness. The curves are shifted for clarity.

[15]. It needs a uniform sample to observe this difference, which is not resolved in the relatively broad peak of Fig. 2. In Ref. [7], SAXS from a uniform sample confirmed the interpretation as perforated lamellae of AFM images very similar to Fig. 3(a). Because we did not succeed to obtain a uniform sample in the present case, additional TEM measurements were performed (Fig. 3(b)). Note that unstained samples were used, preventing any possible influence of the staining process on the morphology. The drawback is that the resulting pictures have little contrast and reproduce not very well. Nevertheless, close inspection reveals lines with similar modulations as observed by AFM and again absence of any ‘head-on’ cylinders. We conclude that the TEM results substantiate the interpretation of a HPL phase upon crystallization, though we cannot fully exclude the possibility of a strongly distorted HPC phase.

Cooling down the melt causes an increase in χ leading to stretching of the polymer chains. As a consequence an increase in both the intercylinder distance a and the peak

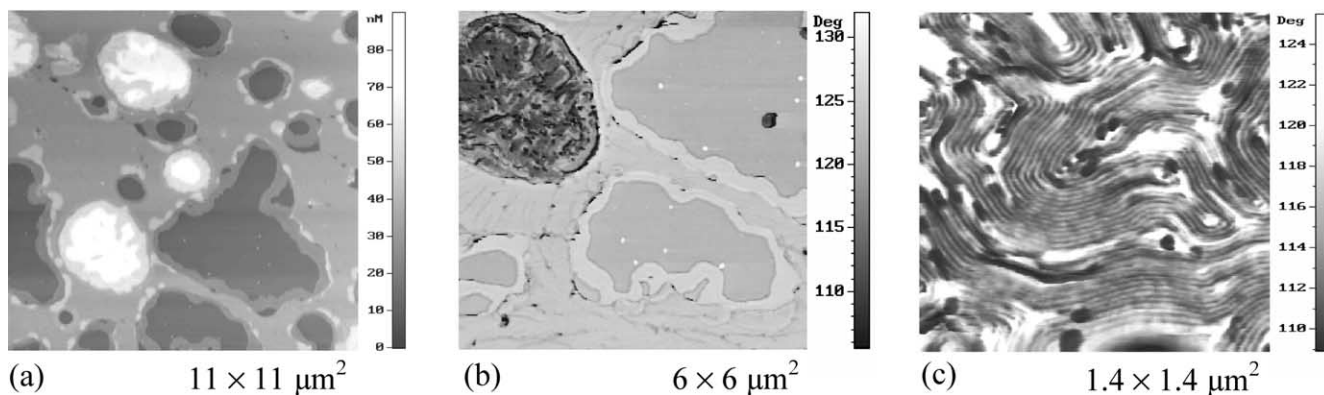


Fig. 5. Tapping mode AFM images of BE37 crystallized at 40°C in films spin-coated from 0.5% DCM solution (sample B). (a) Topography image showing multiple height levels on the surface resembling hole/island structure of lamellar diblock copolymer films. (b) Phase picture revealing difference in the phase contrast between an island (upper left corner) and the rest of the film. (c) Blowup of the island showing lateral phase variations with a period of about 20 nm.

intensity is measured by SAXS. The crystallization of the PEO-block leads to a jump-like increase in χ . At low supercooling the increasing strength of the micro-phase separation is in kinetic competition with the tendency of the crystals to form lamellae. In several cases this has been observed to shift the morphology from HPC to lamellar [1]. Alternatively, this can drive the development of a HPL phase as a compromise between improved cylindrical block ordering and crystalline lamellae [7]. The HPL phase takes the form of alternating PEO and PB_h layers, in which the PEO layers are interrupted by hexagonally arranged PB_h perforations. The HPL phase has been observed at thermally induced phase transitions from a lamellar to a HPC phase [16] and in mechanically sheared samples [17]. Its (meta)stability is still a matter of discussion.

In thin films, additional surface interactions come into play imposing segregation of the components at the interfaces. In lamellar BE films the dissimilar film boundaries dictate wetting PEO and PB_h layers on the substrate and the air interface, respectively [9]. As a result the thickness of the film equals $(n+0.5)L$, where L is the lamellar repetition period and n an integer. While any cross-section parallel to the lamellae exhibits the same symmetry as a planar surface, this is not the case in cylinder-forming systems. In the latter case a planar surface always breaks the symmetry of the bulk structure and the micro-domain phase has to adjust. Hence, a variety of deviations from the bulk morphology has been observed near surfaces and in thin films, such as wetting layers, perforated lamellae, and lamellae, which have been identified as surface reconstructions (see Refs. [18, 19]). For dissimilar interfaces hybrid structures have been found and successfully modelled [18]. AFM images from the crystallized BE37 films A and B (Fig. 5) indicate at the surface wetting layers. We assume that in particular the affinity of the PEO-block for the silica surface drives the formation of parallel lamellae. The effect of the surface field persists over three layers in sample B (Fig. 5(a)) unlike the predicted decay length of about one period [18]. Apparently, for a certain film thickness both the substrate and the air interfaces act coherently and cause parallel alignment over several layers. Yet in the interior of the thicker films C and D the bulk morphology should be preserved. Combining these two aspects we assume that in the melt of thick BE37 films homogeneous wetting layers orient the cylinders in the central part of the films parallel to the substrate. Thus alternating quasi-layers of PEO cylinders surrounded by PB_h and pure PB_h regions will be formed. This model implies a terrace height ΔL of the order of the average bulk repetition period $L=2\pi/q_{100}$. Indeed, $L=18.1$ nm at 90 °C is comparable to the height difference $\Delta L=18$ –19 nm given by the beating in the X-ray reflectivity (Fig. 6).

To check the structure discussed, we modelled the density profile of the molten sample C in various ways. As starting point we represented the PEO cylinders embedded in the rubbery PB matrix by four consecutive layers parallel

to the surface with a thickness $L\approx 18$ nm. Each of them consisted of sublayers of pure PB (matrix) and of mixed PB/PEO (embedded cylinders). The density of the latter layers was taken as a weighted average of the densities of the pure components. In addition we introduced half a wetting layer ($L/2$) of PEO at the substrate, bringing the total to 4.5 layers contributing to the film thickness. The resulting reflectivity curve had many orders of Bragg peaks not observed in the experimental data. Subsequent variation of the density of the layers, the roughness and the period did not lead to significant improvement. A reasonable fit (Fig. 7(a)) could only be obtained by modifying the slab close to the air interface taking instead of mixed PB/PEO (as in the ‘bulk’ of the film) a pure PEO sublayer (Fig. 7(b)). This leads to some redistribution of the PEO cylinders in the PB matrix disturbing the regular periodicity. Note that the results in Fig. 7(a) are displayed as R/R_F on a logarithmic scale, highlighting the deviations from a perfect fit rather than the qualities of the fitting. In order to take the different height levels on the surface into account we simulated two curves for films with 4.5 and 3.5 layers. By adding them incoherently with a weigh factor w we obtained the fit shown in Fig. 7(b). For the 3.5-layer film we used $\Lambda=67.4$ nm and $w=0.35$, and for the 4.5-layer film $\Lambda=86.2$ nm and $w=0.65$. The weight factors imply that, on average, the top layer consists of 65% elevations and 35% depressions and the total film thickness is quantized as $(n+0.5)L$ with $L=19\pm 1$ nm. The results for the 4.5-layer film are summarized in Table 2. They show somewhat low values for the thickness of the PB/PEO sublayer and high ones for the pure PB sublayer. We attribute this to the interlayer roughness that is of the order of several nanometers. The results indicate a variation in L from layer to layer with the period in the interior of the film being close to the bulk one. Hence though layering is involved there is no repetition that would lead to Bragg reflections.

We applied the same model and fitting procedure to the other reflectivity curves from the melt. A fit of sample D with 7.5 layers gave $\Lambda=142$ nm and average period of 19 nm. The values of the parameters essentially confirm the results from the 1% sample. For the thinner films A and B different parameters of the cylindrical and lamellar layers along the limiting interfaces were needed. Moreover, due to the uneven surface coverage, several layers with different characteristics had to be added. As anticipated from the earlier discussion, because of the difference in interior structure the parameters of thicker films were not directly suitable to fit the curves of the thinner ones. Upon crystallization the reflectivity curves smear due to roughening of the air/film interface and show no additional features. For samples A and B a model with a lamellar layer covering the surface of the film is not applicable as the AFM pictures show lateral phase variation that coexist with laterally homogeneous layers. In the bulk BE37 the HPC phase transforms to HPL, which, depending on the amount of supercooling, leads to a 10–50% increase in

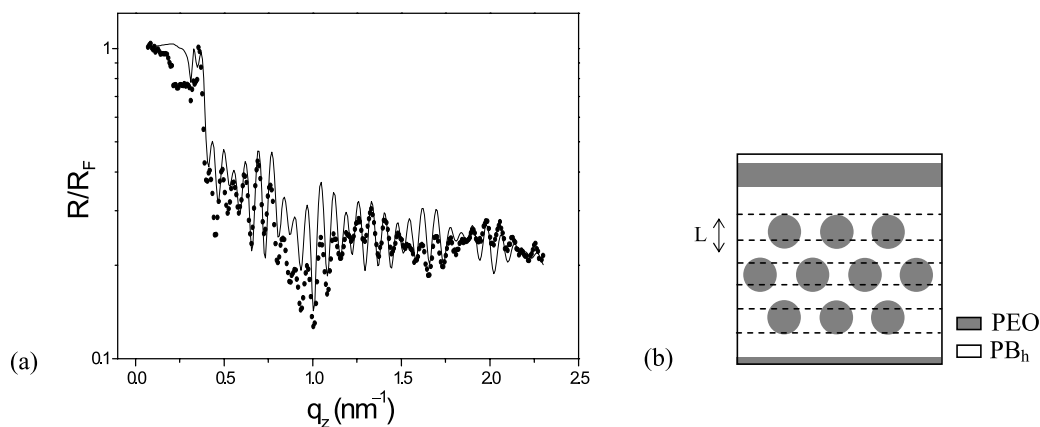


Fig. 7. Modelling of the X-ray reflectivity of film C of BE37 in the melt at 90 °C. (a) Reflected intensity divided by the Fresnel reflectivity R_F and corresponding fit (full line). (b) Model of a cross-section of the thin film morphology.

the period. The same phenomenon should lead to an increase in the film thickness but the quality of the fringes in the experimental XR curves does not allow an unambiguous direct estimate.

Combination of all experimental results indicates for films of BE37 a hybrid melt morphology. The surface affinity of the copolymer blocks drives the formation of wetting layers on the top (PB_h) and bottom (PEO) interfaces. As a result, in the interior of the thicker films PEO cylinders tend to orient parallel to the surface. This hybrid morphology complicates the discussion of the subsequent PEO crystallization, and does not seem to allow a simple model for understanding perpendicular crystalline lamellae we have been looking for. Nevertheless, let us compare our results and the original observations in Refs. [10,11], in which the authors associate the presence of terraces on the film surface with a lamellar structure parallel to the substrate. Our results indicate that the morphology in the interior of the thicker films differs from the top and bottom interfaces. Moreover the AFM images (Fig. 5) unequivocally show a hybrid crystalline morphology for the thinner films. In Refs. [10,11], the crystallization is assumed to be connected to a decrease in d_{PEO} , the PEO sublayer thickness. The associated lateral expansion is supposed to be difficult to accommodate, leading in thin films to vertical

lamellae ('escape into the third dimension'). However, from the work of Opitz et al. [9] we know that in lamellar films d_{PEO} increases upon crystallization to accommodate the nearest (half) integer number of stems. In uniform lamellar films this is accompanied by lateral contraction, leading to cracks through the whole film. In the present case the crystallization might start from the wetting layers at the interfaces that are necessarily most stretched. The strain in the wetting layers and the hybrid morphology now can probably serve to accommodate any contraction upon crystallization. Note that for crystallization inside a PEO cylinder the diameter of the cylinder (about 13.5 nm) can neither accommodate a non-folded PEO chain of 18.5 nm nor a series of (half)integer folded chains. Orientation of the stems along the cylinder axis (crystal lamellae perpendicular) would not lead to such restrictions and might be favoured. For cylinders parallel to the substrate this allows the possibility of crystalline lamella perpendicular to the substrate, even though other possibilities are not excluded. Further, modelling should include the interaction between PEO in the cylinders and in the wetting layer near the surface, which seems to be prohibitively difficult. Due to the complicated hybrid structures the final result is expected to depend strongly on the detailed experimental conditions, as is indeed observed.

Table 2
Fitting parameters for a 4.5-layer film (sample C)

| Slab | Composition | Density ($10^{-3} \text{ e}^- \text{ nm}^{-2}$) | d (nm) | L (nm) | Roughness (nm) |
|------|-------------|--|----------|----------|----------------|
| 1 | PB | 8.87 | 4.60 | | 1.1 |
| 2 | PEO | 10.33 | 9.50 | 21 | 1.5 |
| 3 | PB | 8.87 | 11.5 | | 0.9 |
| 4 | PEO/PB | 9.38 | 9.50 | 18.8 | 1.1 |
| 5 | PB | 8.87 | 9.30 | | 1.7 |
| 6 | PEO/PB | 9.35 | 9.50 | 18.2 | 1.4 |
| 7 | PB | 8.87 | 8.70 | | 1.5 |
| 8 | PEO/PB | 9.25 | 11.2 | 20.3 | 1.0 |
| 9 | PB | 8.87 | 9.10 | | 1.0 |
| 10 | PEO | 10.44 | 3.25 | | 1.0 |

5. Conclusions

We have studied the bulk and thin film morphology of a asymmetric block copolymer BE37, using simultaneous SAXS/WAXS, X-ray reflectivity, optical microscopy, AFM and TEM. In the bulk, the melt morphology of HPC most probably transforms into a HPL phase upon crystallization. In thin films wetting layers of PB_h and PEO develop at the top and bottom interfaces, respectively. In the melt of BE37, these layers force the cylinders in the interior of the film to orient parallel to the substrate. The crystallization of the PEO block giving perpendicular lamellae cannot be ascribed to a simple process. Because of the complicated hybrid structures, the final result can vary in dependence of the history and associated kinetic pathways and in general lateral structures develop coexisting with lamellar layers in thinner films.

Acknowledgements

We thank P.H.H. Bomans (Maastricht) for carrying out the TEM measurements. This work is part of the Softlink research program of the ‘Stichting voor Fundamenteel Onderzoek der Materie (FOM)’, which is financially supported by the ‘Nederlandse Organisatie voor Wetenschappelijk Onderzoek (NWO)’.

References

- [1] See for example Hamley IW. *The Physics of block copolymers*. New York: Oxford University Press; 1998.
- [2] DiMarzio EA, Guttman CM, Hoffman JD. *Macromolecules* 1980;13:1194.
- [3] Whitmore MD, Noolandi J. *Macromolecules* 1988;21:1482.
- [4] Vilgis T, Halperin A. *Macromolecules* 1991;24:2090.
- [5] (a) Zhu L, Chen Y, Zhang A, Calhoun BH, Chun M, Quirk RP, et al. *Phys Rev B* 1999;60:10022.
(b) Zhu L, Cheng SZD, Calhoun BH, Ge Q, Quirk RP, Thomas EL, et al. *J Am Chem Soc* 2000;122:5957.
- [6] (a) Loo Y-L, Register RA, Ryan AJ. *Macromolecules* 2002;35:2365.
(b) Loo Y-L, Register RA, Ryan AJ, Dee GT. *Macromolecules* 2001;34:8968.
- [7] Li L, Serero Y, Koch MHJ, de Jeu WH. *Macromolecules* 2003;36:529.
- [8] de Jeu WH. In: Reiter G, Sommer J-U, editors. *Polymer crystallization: observations, concepts and interpretations*. Berlin: Springer; 2003. p. 196–207 [Springer Lecture Notes in Physics; 606].
- [9] Opitz R, Lambrea DM, de Jeu WH. *Macromolecules* 2002;35:6930.
- [10] Reiter G, Castelein G, Hoerner P, Riess G, Blumen A, Sommer J-U. *Phys Rev Lett* 1999;83:3844.
- [11] Reiter G, Castelein G, Hoerner P, Riess G, Sommer J-U, Floudas G. *Eur Phys JE* 2000;2:319.
- [12] (a) See for example Tolan M. *X-ray scattering from soft-matter thin films*. Springer Tracts Mod Phys 1999;148.
(b) Holý V, Pietsch U, Baumbach T. *High-resolution X-ray scattering from films and multilayers*. Springer Tracts Mod Phys 1999;149.
- [13] Leibler L. *Macromolecules* 1980;13:1602.
- [14] Harrison C, Park M, Chaikin PM, Register RA, Adamson DH, Yao N. *Polymer* 1998;39:2733.
- [15] Förster S, Khandpur AK, Zhao J, Bates FS, Hamley IW, Ryan AJ, et al. *Macromolecules* 1994;27:6922.
- [16] (a) Hamley IW, Koppi KA, Rosedale JH, Bates FS, Almdal K, Mortensen K. *Macromolecules* 1993;26:5959.
(b) Hajduk DA, Gruner SM, Rangarajan P, Register RA, Fetters LJ, Honeker C, et al. *Macromolecules* 1994;27:490.
- [17] (a) Qi S, Wang ZG. *Macromolecules* 1997;30:4491.
(b) Hajduk DA, Takenouchi H, Hillmyer MA, Bates FS, Vigild ME, Almdal K. *Macromolecules* 1997;30:3788.
- [18] Lyakhova KS, Sevink GJA, Zvelindovsky AV. *J Chem Phys* 2004;120:1127.
- [19] Knoll A, Horvat A, Lyakhova KS, Krausch G, Sevink GJA, Zvelindovsky AV, et al. *Phys Rev Lett* 2002;89 [035501-1].